3B.9

THE POTENTIAL FOR ESTIMATING CLOUD LIQUID WATER PATH OVER SEA ICE FROM AIRBORNE PASSIVE MICROWAVE MEASUREMENTS

Julie A. Haggerty[!] and Judith A. Curry
Program in Atmospheric and Oceanic Sciences
University of Colorado
Boulder, Colorado

1. Introduction

Potential effects of global warming on the polar sea ice have heightened interest in understanding the factors which control polar atmospheric, oceanic, and ice processes. Expanding our knowledge of cloud processes, particularly in the data-sparse Arctic region, is important for improving model predictions. On an operational level, cloud cover may produce spurious results in sea ice concentration estimates. Despite the need for understanding the complexities of arctic cloud processes, little observational cloud data is available. Satellite retrieval techniques, which provide information about clouds over other remote areas of the world, encounter difficulties in polar regions due to the fact that Arctic clouds are frequently low-level and optically thin. Given the high albedo of the snow/ice surface, there is little contrast between clouds and surface in the visible part of the spectrum. Since the clouds are low, their temperatures tend to be close to that of the surface, so there is little thermal contrast as well. Microwave emissivities of the sea ice surface are high and variable, so arctic clouds containing small amounts of liquid or ice water do not have a large effect on the microwave signal, especially at lower frequencies. To further investigate some of these issues, aircraft observations were conducted as part of the FIRE Arctic Clouds Experiment (FIRE-ACE) in conjunction with the Surface Heat Budget of the Arctic (SHEBA) experiment (Curry et al., 2000; Perovich et al., 1999)

Passive microwave measurements from satellites have been used in other parts of the world for estimating cloud properties such as liquid water path, ice water path, and precipitation rate. Most retrievals are performed over ocean surfaces where the low, uniform surface emissivity provides significant contrast with overlying clouds (e.g., Liu and Curry, 1993; Kummerow et al., 1996). Liquid water path (LWP) retrievals over land have also been attempted using passive microwave data (Greenwald et al., 1997). Cloud retrievals over sea ice encounter similar challenges as those over land, namely the separation of the cloud signal from emission by a radiometrically warm surface that may experience frequent

changes in its dielectric properties. Thus there have been no attempts to date to relate cloud liquid or ice water path to satellite microwave radiances over sea ice. Model simulation studies suggest, however, that in some circumstances the cloud LWP signal is significant at frequencies of 85-90 GHz, and is discernible against the bright sea ice background (Liu and Curry, 2001).

In this study we examine the feasibility of retrieving cloud LWP over sea ice using measurements from SHEBA and FIRE-ACE. Using airborne passive microwave data and radiative transfer model simulations, we attempt to identify the optimal frequencies for LWP retrieval and to estimate minimum detectable levels of LWP over sea ice and probable accuracies of the estimates.

2. Data Sets

2.1 Field Experiment

The Surface Heat Budget of the Arctic (SHEBA) experiment was conducted from October 1997 to October 1998 in the Beaufort and Chukchi Seas (Perovich et al. 1999). The Canadian Coast Guard icebreaker Des Groseilliers served as a base camp to deploy a variety of sensors to measure ice, snow, and meteorological properties. In conjunction with the SHEBA effort, the FIRE Arctic Clouds Experiment (FIRE-ACE) extended the spatial domain of SHEBA with aircraft observations of atmospheric and surface properties near the Des Groseilliers (Curry et al., 2000). Aircraft measurements in the vicinity of the SHEBA ice camp were conducted in the spring and summer of 1998. Of particular interest for this work are flights by the National Center for Atmospheric Research (NCAR) C-130 aircraft and the NASA ER-2 aircraft, since both carried microwave radiometers. The NCAR C-130 performed 8 research flights in May and 8 in July of that year. The NASA ER-2 flew 11 missions in May and June.

2.2 Instrumentation

The Airborne Imaging Microwave Radiometer (AIMR) is a cross-track scanning system which flies on the NCAR C-130. Four channels measure upwelling radiation at two frequencies, 37 and 90 GHz, and two orthogonal polarizations which can be converted to horizontal and vertical components.The AIMR views underlying scenes over an angular swath of 120 °. Beam widths of 1 ° at 90 GHz and 2.8 ° at 37

---

[1] Corresponding author address: Julie A. Haggerty, National Center for Atmospheric Research, P.O. Box 3000, Boulder, CO 80304: email: haggerty@ucar.edu

GHz produce spatial resolutions on the order of 20 m to 300 m at typical flight altitudes and velocities. Corresponding swath widths are approximately 3-20 km. Detailed specifications for the AIMR can be found in Collins et al. (1996)

The Millimeter Imaging Radiometer (MIR) was flown on the NASA ER-2 during FIRE-SHEBA. The MIR is a cross-track scanner measuring microwave radiation at several frequencies, including 89, 150, and 220 GHz. It scans over an angular swath of 100 ° and has a 3.5 ° beam width. Resulting swath width at the typical 20 km flight altitude of the ER-2 is approximately 48 km. Separation of the vertically and horizontally polarized components is not possible with this instrument, so mixtures of brightness temperature components are used.

3. Model Simulations

To understand the response of AIMR and MIR measurements in an arctic environment, numerical simulations of top-of-atmosphere (TOA) brightness temperatures (T_B) were conducted for conditions approximating those observed during spring and summer around the SHEBA site. The model used to simulate T_B values is a plane-parallel microwave radiative transfer model (Liu, 1998). In the model, absorption coefficients for atmospheric gases (water vapor and oxygen) are calculated according to Liebe and Layton (1987). Absorption and scattering coefficients and phase functions for condensed water and ice are calculated using Mie theory. The complex refractive indices of liquid water are taken from the empirical formulations of Ray (1972). Refractive indices for ice are from Warren (1984). As noted by Lin et al. (1998) there are no measurements to support the liquid water parameterizations at cloud temperatures below 258 K, and significant disagreement exists between the Ray parameterizations and Liebe et al. (1991) parameterizations for supercooled water. Given the insufficient number of measurements to support a specific parameterization at supercooled temperatures, we use the Ray parameterizations following Liu and Curry (1993), Lin et al. (1998), and others.

A series of baseline cases representing observed conditions during FIRE-SHEBA has been defined for these simulations. Atmospheric profiles of temperature and water vapor from aircraft measurements are used as model input up to flight levels of about 6 km. Above that level, standard profiles representing summer sub-Arctic conditions are blended with the measured profiles. Cloud heights and temperatures are also derived from the aircraft profiles. Surface emissivity values are based on estimates from Haggerty and Curry (2001). Surface temperatures are estimated from aircraft infrared radiometer measurements (Haggerty and Curry, 2001).

Model runs described here focus on non-precipitating liquid phase clouds with droplet radii smaller than 100 μm. Liquid water path is varied over a range suggested by in situ aircraft measurements of liquid water content and ground-based measurements from a 31 GHz microwave radiometer (Y. Han and E. Westwater, personal communication, 2000). Based on these measurements, we vary LWP over a range of 0-200 g m^{-2} in May and 0-500 g m^{-2} in July. Although higher values are occasionally observed by the ground-based microwave radiometer, our simulations are based largely on aircraft data which falls within these ranges. In addition, ground-based radiometer estimates of LWP fall outside this range infrequently (e.g., in the presence of precipitation).

Four cases are examined to represent the range of conditions seen during FIRE-SHEBA in May and July. The properties of each case are listed in Table 1. The cases comprise a range of cloud heights and temperatures which are derived from aircraft profiles. To simplify the interpretation of the effect of cloud temperature on TOA brightness temperatures, the profiles are idealized so that each cloud layer is isothermal. Cloud temperature is derived by simply averaging the temperature profile through the cloud layer. Cloud temperatures are below freezing in May and near freezing and above in July. Clouds are assumed to contain no ice particles for the initial simulations. Surface emissivities calculated from proximate clear sky days are used in the model simulations. May emissivity values are representative of a dry snow layer covering the multiyear ice (Haggerty and Curry, 2001). Low emissivity values at 90 GHz and 150 GHz are found to result from volume scattering by the snow layer. Melting conditions in July raise the emissivity at 90 GHz. Simulations are performed for horizontal polarizations at 37 and 90 GHz, since the lower emissivity at high viewing angles should provide better contrast between surface and atmosphere. Since the MIR sensor mixes polarizations, we are unable to separate horizontal and vertical component and have therefore simply used an average value of emissivity at 150 GHz and 220 GHz. Note that MIR data is not available in July, so only 37 GHz and 90 GHz are considered in the July simulations.

Table 1: Specifications for MWRT simulations

Date (case)	Surface Temperature (K)	Cloud Height (m)	Cloud Temperature (K)	Precipitable Water (kg m^{-2})
May 15 (a)	264.1	100-400	264.8	5.8
May 27 (b)	272.2	100-500/1300-1500	270.6 / 271.9	12.6
July 18 (c)	273.2	0-100 2000-3500	276.2 269.5	22.7
July 29 (d)	273.2	100-500	270.5	12.2

3.1 Brightness Temperature Variations

Results of model simulations are presented in Figure 1 which shows T_B as a function of LWP for each case. In all cases we see an increase in T_B over the range of LWP considered. The magnitude of the changes, however, varies substantially between frequencies. In case (a), the effect of increasing LWP is largest at 90 GHz and 150 GHz with ΔT_B of 27-29 K. A higher surface emission term coupled with lower liquid water emission at 37 GHz produces little change at that frequency in these conditions. The T_B variation is also small at 220 GHz where the surface emission is higher and atmospheric water vapor emission is larger than at the lower frequencies. Variations are similar in case (b), although higher surface temperature and atmospheric water vapor burden raise the baseline (no liquid water) value of T_B at all frequencies. The resulting ΔT_B values at both 90 GHz and 150 GHz are lower in case (b) due to higher background T_B. The higher cloud temperatures compared to case (a) may also contribute to the reduced LWP signal. The absorption coefficient of liquid water decreases with increasing temperature, so the emissivity of a warmer cloud is lower than that of a colder cloud (although the variation for supercooled water has not been documented). The higher emitting temperature of the cloud serves to increase the total emission, however, so this effect offsets the reduction in cloud emissivity. In this case, it is not clear which effect is dominant.

The summertime cases (c and d) also exhibit steady increases in T_B with increasing LWP. Surface conditions at this time tend to reduce the contrast between surface radiation and atmospheric radiation. Emissivity is higher for melting ice and surface temperatures are significantly warmer. Higher water vapor levels, as seen in case (c), also contribute to higher background T_B values. Therefore in cases (c) and (d) we see 90 GHz ΔT_B values on the order of 15 K and 20 K, respectively.

Based on this analysis, it appears that the 90 GHz (horizontal) signal contains the most information about LWP values in the conditions encountered during FIRE-SHEBA. Conditions for which liquid water produces the largest ΔT_B are those with lower surface emission, i.e., low physical temperatures and/or low emissivity. Emissivity at 90 GHz tends to be lower for dry snow and higher for summer melt conditions (Haggerty and Curry, 2001). Physical temperatures warm as summer approaches. Therefore it would appear that springtime (snow-covered) conditions provide a better opportunity for accurate estimations of liquid water path. Higher LWP values in the summer may compensate for the reduction in contrast due to higher surface emission.

4. Liquid Water Path Retrieval

We apply the method of Liu and Curry (1993) for estimation of LWP. Their method relates LWP to the liquid water absorption coefficient at a given frequency, the cloud emissivity, and the viewing angle. Cloud emissivity is shown to depend on T_B, the cloud brightness temperature at a given frequency; T_{B0}, the corresponding clear-sky brightness temperature which accounts for emission from the surface and atmospheric water vapor; T_C, the cloud mean temperature;
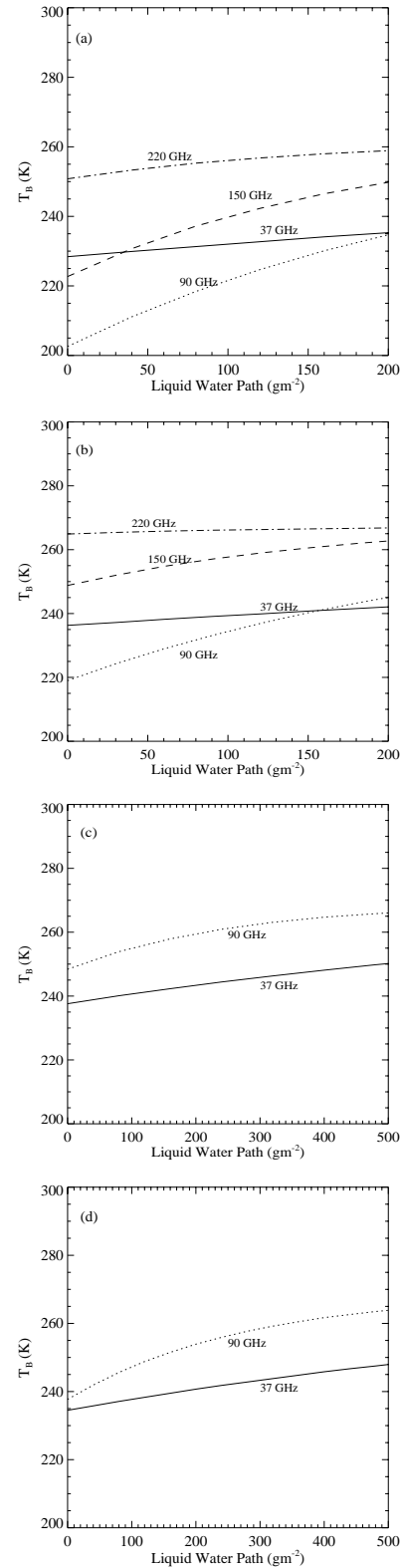
Figure 1: Simulated brightness temperatures for the cases described in Table 1
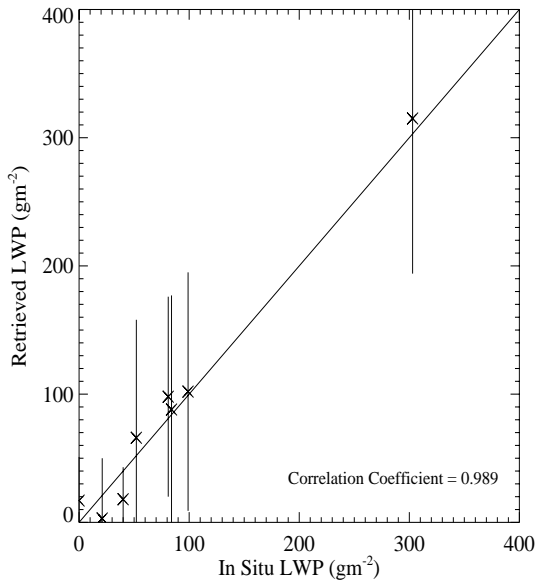
Figure 2: Comparison of LWP retrieved from passive microwave measurements with LWP calculated from in situ measurements of liquid water content along an aircraft slant profile

T_A, the mean air temperature; and T_S, the surface temperature. In our implementation of the Liu and Curry algorithm, T_A, and T_C are obtained from aircraft profiles through the observed cloud layer. T_S is measured by the infrared radiometers during flight segments under the cloud, and T_B is measured by the microwave radiometers. T_{B0} is constructed using the Liu (1998) microwave radiative transfer model with input from aircraft temperature and humidity profiles, surface temperature, and surface emissivity as estimated in Haggerty and Curry (2001) We use brightness temperatures at 90 GHz (horizontal polarization) based on results of model simulations.

We consider seven cases with clouds observed on flights during May and July, 1998. The cases represent a range of cloud depths, liquid water contents, phase, and temperature. LWP estimates from the AIMR 90 GHz (horizontal polarization) channel are compared with LWP values derived from aircraft measurements of LWC. Since the aircraft slant profiles cover a significant horizontal distance, we cannot compare LWP at a single location. Therefore we calculate the mean LWP retrieved from AIMR over the extent of the observation area (typically 50 x 50 km centered on the SHEBA ship) and compare it with the integrated aircraft liquid water profile. The comparisons for all cases are shown in Figure 2. Among these cases, we see LWP values that range from near zero to 300 g m^{-2}. The correlation between retrieved LWP and in situ values is 0.989 with an RMS error of 14 g m^{-2}. Absolute and relative errors are largest at small values of LWP. For example, on May 15 the mean retrieved LWP is 3 g m^{-2} while the in situ LWP is 21 g m^{-2}. The mean retrieved LWP on May 18 is 18 g m^{-2} and the in situ LWP is 40 g m^{-2}. These results are not unexpected since uncertainties in surface emissivity have a large influence at low liquid water amounts, whereas for high LWP values the surface influence is less apparent. As we move to higher LWP values, we see that the agreement between retrieved and in situ values improves. The cases analyzed here suggest that 50-60 g m^{-2} may be a lower limit for detectability by this algorithm.

5. Summary

Model simulations of upwelling brightness temperature in arctic conditions have been used to demonstrate that liquid water clouds produce detectable increases in brightness temperature, and that the magnitude of the increase is proportional to LWP. Brightness temperatures at 90 GHz show the largest response to LWP for the conditions considered when compared to responses at 37 GHz, 150 GHz, and 220 GHz.

An algorithm developed for estimation of LWP over oceans using SSM/I data has been adapted for use over sea ice with airborne microwave radiometer data. The algorithm has been applied to seven cases observed during the FIRE-SHEBA aircraft campaigns. Retrieved values of LWP have been compared to aircraft in situ measurements with mixed results. Agreement between the two data sets is very good at high LWP values (100 g m^{-2} and above). Discrepancies are largest at very low LWP (< 50 g m^{-2}) where the magnitude of brightness temperature variations due to surface emissivity uncertainties is comparable to the cloud liquid water signal. Further results will be described at the conference

6. References

Collins, M.J., F.G.R. Warren and J.L. Paul, 1996: Airborne imaging microwave radiometer -- Part I: Radiometric analysis, *IEEE Trans. Geosci. Rem. Sens.*, **34**(3), 643-655.

Curry, J.A., P. Hobbs, M. King, D. Randall, P. Minnis et al., 2000: FIRE Arctic clouds experiment, *Bull. Amer. Met. Soc.*, **81**(1), 5-29

Haggerty, J.A., and J.A. Curry, 2001: Variability of surface emissivity estimated from airborne passive microwave measurements during FIRE SHEBA, *J. Geophys. Res.*, in press.

Liebe, H.J. and D.H. Layton, 1987: Millimeter wave properties of the atmosphere: Laboratory studies and propagation modeling, National Telecommunications and Information Administration (NTIA) Report 87-24, 74pp.

Lin, B., P. Minnis, B. Wielicki, D.R. Doelling, R. Palikonda, D.F. Young, and T. Uttal, 1998: Estimation of water cloud properties from satellite microwave, infrared and visible measurements in oceanic environments: 2. Results, *J. Geophys. Res.,* **103**, 3887-3905.

Liu, G., 1998: A fast and accurate model for microwave radiance calculations, *J. Meteorol. Soc. Jpn.,* **76**(2), 335-343.

Liu, G., and J.A. Curry, 2001: Observation and interpretation of microwave hot spots over the Arctic Ocean during winter, submitted to *J. Geophys. Res*.

Liu, G., and J.A. Curry, 1993: Retrieval of characteristic features of cloud liquid water from satellite measurements, *J. Geophys. Res.,* **98**, 5069-5092.

Perovich, D.K., E.L. Andreas, J.A. Curry et al.: Year on ice gives climate insights. *EOS*, 80, 481, 1999a.

Ray, P.S., Braodband complex refractive indices of ice and water, *Appl. Opt., 11*, 1836-1844, 1972.